



New bisoliton solutions in dispersion managed systems

M. Shkarayev*, M.G. Stepanov

Department of Mathematics, The University of Arizona, 617 N. Santa Rita Ave., Tucson, AZ 85721, USA

ARTICLE INFO

Article history:

Received 29 November 2007

Received in revised form

2 December 2008

Accepted 2 February 2009

Available online 4 March 2009

Communicated by J. Bronski

Keywords:

Dispersion management

Bisoliton

Iterations convergence

ABSTRACT

In this paper we propose a method which provides a full description of solitary wave solutions of the Schrödinger equation with periodically varying dispersion. This method is based on analysis and polynomial deformation of the spectrum of an iterative map. Using this method we discover a new family of antisymmetric bisoliton solutions. In addition to the fact that these solutions are of interest for nonlinear fiber optics and the theory of nonlinear Schrödinger equations with periodic coefficients, they have potential applications for increasing of bit-rate in high speed optical fiber communications.

© 2009 Elsevier B.V. All rights reserved.

1. Introduction

Chromatic dispersion of optical fibers is one of the major factors limiting the capacity of fiber communication systems. It results in broadening of optical pulses due to differences in velocities of different spectral components. The dispersion management technique [1] was proposed as a method to solve the problem of dispersive pulse broadening. An optical fiber link with dispersion management is composed of periodically arranged fiber spans with alternating signs of dispersion. The fiber spans are chosen to make the cumulative effect of dispersion small or even zero. Full compensation of the dispersive effects is achieved by making the mean value of the dispersion to be zero. In this case as a pulse propagates over one period it will be spread and then contracted to its original shape.

Increasing bit-rates inevitably leads to manifestation of nonlinear properties of optical fibers. As bit rates increase, the temporal width of an optical pulse (bit carrier) τ_0 decreases. On the other hand the energy of the pulse must remain above some critical level $\mathcal{E} \geq \mathcal{E}_{cr}$ to provide minimal detection bit-error at the end of the line, and therefore the power of the signal ($P \sim \mathcal{E}/\tau_0$) increases as the pulse narrows $P \geq \mathcal{E}_{cr}/\tau_0$. It is a well known, experimentally verified fact that the index of refraction of the fiber core grows linearly with the power of the signal, $n = n_0 + \alpha P$ (where n_0 is linear index of refraction and α is a coefficient of Kerr

nonlinearity). With a high enough power the nonlinear response of the medium becomes important. Since dispersion management is a purely linear approach to compensate for pulse broadening, the validity of this approach becomes less obvious in the presence of nonlinearity. It was shown that in presence of nonlinearity the compensation is still possible for a special class of pulses known as the dispersion managed (DM) solitons [2]. Detailed information about the DM solitons and their applications can be found in [3].

Soon after the concept of DM solitons was introduced, it became clear that both analytic representation and accurate numerical description of the DM soliton shape are challenging problems. The first problem was addressed in many papers, where approximations of the central part of the DM soliton and asymptotic of oscillatory tails was considered (see [4–6]). However the general solution of this problem remains unsolved. The problem to determine an accurate numerical description of the DM soliton shape was solved by in [7–9] using a slow dynamics model of DM solitons proposed in [10]. Later this approach was used to address the behavior of DM solitons for the systems with both dispersion and nonlinearity compensation [11].

The dispersion compensation while resolving the physical problem with the pulse broadening, poses an obstacle for the numerical computation of such solutions. Following the standard approach, the description of a soliton consists of launching a signal and waiting for all the continuous radiation to escape. For the problem with dispersion management this process is extremely slow and ineffective on the tails of the soliton. Authors of [7] proposed solving the averaged equation for the analysis of solutions, which for the solitary waves reduces from an integro-differential equation to a nonlinear integral equation, solvable by a nonlinear iterative procedure. This allowed for a fast way of

* Corresponding address: Department of Mathematics, The University of Arizona, 617 N. Santa Rita Ave., P.O. Box 210089, Tucson, AZ 85721, USA. Tel.: +1 520 360 7871.

E-mail address: max@math.arizona.edu (M. Shkarayev).

achieving precision exceeding any necessary requirements for the practical applications.

Unlike the conventional NLS soliton, the dispersion managed system supports propagation of bound pairs of solutions, or bisolitons. Existence of bisoliton solutions was shown in the numerical investigations of [12] and later confirmed experimentally in [13]. It should be noted that this experimental work considered antisymmetric bisolitons and therefore we limit our investigation to this type of bisoliton. These solutions are interesting for the theory of nonlinear partial differential equations, and represent a new phenomenon in nonlinear fiber optics. They illustrate a new type of solution of a nonlinear Schrödinger equation where the dispersion coefficient is replaced with a periodic function. The potential applications for the optical communication systems were discussed in [13]. Bisolitons can be used to introduce a three-letter alphabet (“empty slot”, “DM soliton” and “bisoliton”), replacing a conventional binary alphabet. This could increase the system capacity without a change to the physical parameters of the system.

The shape as well as other important characteristics of bisolitons were found in [14] using a modification of the numerical method proposed in [7–9]. The equation describing averaged dynamics of the solution is reduced to have a single universal parameter, which incorporates all of the physical and geometrical characteristics of the optical system [14]. Analysis of this equation showed the existence of two branches of bisoliton determined by the universal parameter, with a critical bifurcation point connecting the two branches.

Investigation of DM bisolitons was based on the iteration of a nonlinear map. The analysis of the newly discovered branch of solutions was complicated by the lack of convergence of the iterative procedure. Careful analysis of the map showed the existence of eigenvalues outside of the unit circle, explaining the existence of the growing modes of the map. In this work we propose to utilize the method of polynomial spectral transformations to construct a contractive map, preserving the original fixed points. The application of this method allowed for the discovery of the previously unknown branch of bisoliton solutions. These bisolitons present new solutions to nonlinear Schrödinger equation with periodic dispersion. A recent paper [15] indicates new experimental evidence for the existence of this branch of bisoliton solutions. These newly found bisoliton solutions allow for the introduction of a 4-letter alphabet, further increasing the capacity of existing lines.

2. Basic equations

A well established model for the propagation of an electromagnetic pulse through a nonlinear, dispersive medium is the nonlinear Schrödinger equation

$$iu_z + d(z)u_{tt} + \gamma|u|^2u = 0 \quad (1)$$

where the scalar function $u(z, t)$ is the envelope of the signal, z is the distance along the fiber, t is retarded time. Without loss of generality we consider a fiber link with constant nonlinearity given by γ . Function $d(z)$ is the dispersion as a function of distance along the fiber. For a dispersion managed system this is a piecewise constant, periodic function which can be written in the form $d(z) = d_0 + d_1$ if $0 < z < L/2$, and $d(z) = d_0 - d_1$ if $L/2 < z < L$, where L is a dispersion map period, and $d_1 \gg d_0$.

A fiber link with dispersion management has a characteristic time scale $\tau_{dm} \equiv (Ld_1/2)^{1/2}$. The physical meaning of this time is the width of a pulse such that the pulse will approximately double in width as it propagates over half of the period. The characteristic “residual dispersion length” $z_{rd} \equiv \tau_{dm}^2/d_0 = Ld_1/2d_0$ is the distance when a pulse with width τ_{dm} propagating over a fiber

with dispersion d_0 will approximately double in width. Rescaling the variables $t = \tau_{dm}\tilde{t}$, $u = 2\pi\sqrt{P}\tilde{u}$ results in the equation

$$i\tilde{u}_z + \frac{2}{L} \frac{d(z) - d_0}{d_1} \tilde{u}_{\tilde{t}\tilde{t}} + \frac{1}{z_{rd}} \tilde{u}_{\tilde{t}\tilde{t}} + (2\pi)^2 \frac{1}{z_{nl}} |\tilde{u}|^2 \tilde{u} = 0. \quad (2)$$

$z_{nl} \equiv 1/(\gamma P)$ is characteristic “nonlinear length” on which the change of the phase of the pulse due to fiber nonlinearity will be of the order 1.

To take advantage of dispersion management in the presence of nonlinearity, the compensation must take place on the distances where nonlinearity effects are small and negligible compared to the local value of dispersion. Therefore the dispersion management works in the linear regime, and two well separated scales of pulse propagation can be distinguished. On the first scale local dispersion will dominate over the weak effects the residual dispersion and the nonlinearity. There the pulse is rapidly broadened and brought back to its original width as a result of the alternating signs of local dispersion. The second scale is where the effects of nonlinearity and residual dispersion accumulate and become important. Thus, the spectrum of the signal can be considered in the form

$$F[\tilde{u}] = q(\Omega, z) \exp\left(-i\Omega^2/(L/2) \int_{L/4}^z d\xi \frac{d(\xi) - d_0}{d_1}\right), \quad (3)$$

with the Fourier transform F defined as $F[f(t)] = \int dt \exp(i\omega t) f(t)$. Here the exponent is the rapidly changing phase due to the large value of local dispersion and the amplitude q is varying slowly with z due to residual dispersion and the nonlinear effects. Substituting this form of \tilde{u} into the Eq. (2) and taking an average over a map period we obtain Gabitov–Turitsyn equation describing evolution of q [10]

$$iq_z - \frac{1}{z_{rd}} \Omega^2 q + \frac{1}{z_{nl}} R(q, \Omega) = 0, \quad (4)$$

$$R(q, \Omega) = \int \frac{\sin(\Delta/2)}{\Delta/2} q(\Omega_1) q(\Omega_2) q^*(\Omega_3) \times \delta(\Omega_1 + \Omega_2 - \Omega_3 - \Omega) d\Omega_1 d\Omega_2 d\Omega_3,$$

where $\Delta \equiv \Omega_1^2 + \Omega_2^2 - \Omega_3^2 - \Omega^2$, and $\delta(\cdot)$ is Dirac’s delta function.

We are interested in computation of antisymmetric bisolitons which are solitary wave solutions of this equation. For such a solution the amplitude profile is independent of the distance along the fiber, and can be written as $q(\Omega, \tilde{z}) = \varphi(\Omega) e^{i\lambda \tilde{z}}$, where λ is a wave number of the solitary wave. With $\lambda = 1/z_{nl}$ the function φ is governed by the following equation

$$\varphi + \bar{d}_0 \Omega^2 \varphi = R(\varphi, \Omega), \quad \text{where } \bar{d}_0 \equiv \frac{z_{nl}}{z_{rd}} = \frac{d_0}{(\gamma P)(d_1 L/2)}. \quad (5)$$

Thus far we have reduced this three parameter partial differential equation to an integral equation with a single free parameter (an alternative way to do that is presented in Appendix A).

3. Solving the integral equation

In this paper we study the family of antisymmetric bisolitons at different positive values of parameter \bar{d}_0 . In order to solve Eq. (5) we use the following iterative procedure [16]

$$\varphi_{n+1} = N_{\bar{d}_0}(\varphi_n), \quad N_{\bar{d}_0}(\varphi) \equiv \mathbb{P}_{\text{odd}} \left(Q^{3/4} \frac{R(\varphi, \Omega)}{1 + \bar{d}_0 \Omega^2} \right) \quad (6)$$

$$Q \equiv \frac{\int |\varphi|^2 d\Omega}{\int |R(\varphi, \Omega)/(1 + \bar{d}_0 \Omega^2)|^2 d\Omega}$$

where Q is a Petviashvili factor [17,18] which is introduced to avoid the convergence to the trivial solution $\varphi = 0$ by

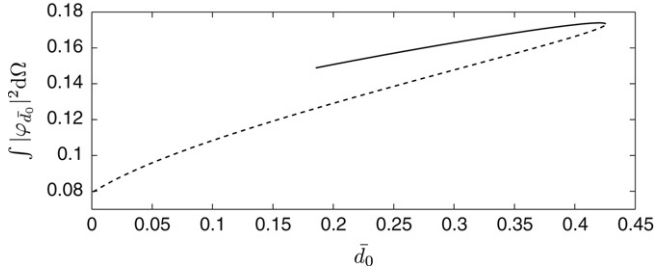


Fig. 1. Energy of the two branches of bisolitons as a function of \bar{d}_0 . The solid line corresponds to the solutions with higher energy (upper branch) and the dashed line corresponds to solutions with lower energy (lower branch).

making that solution unstable. The operator $\mathbb{P}_{\text{odd}}(f(\Omega)) \equiv (f(\Omega) - f(-\Omega))/2$ is a projection onto odd functions, used here to project the iterated functions onto the space of antisymmetric functions. We solve the Eq. (6) numerically, discretizing φ on a grid of M points. The iterations are stopped when φ_n satisfies the condition

$$\|\varphi_n + \bar{d}_0 \Omega^2 \varphi_n - R(\varphi_n, \Omega)\|_{L_2} < 10^{-8}. \quad (7)$$

A Fourier transform of a sum of two Gaussian pulses, shifted apart and taken with opposite signs is used as a seed for the iteration procedure with $\bar{d}_0 = 0.2$. The value of \bar{d}_0 is decreased incrementally, with a previous solution used as a seed for the next value of \bar{d}_0 , until the parameter reaches zero. The same procedure was performed in the increasing direction from $\bar{d}_0 = 0.2$. We found two branches of bisoliton solutions. Fig. 1 shows the energy of the solutions as a function of \bar{d}_0 . The solutions bifurcate near $\bar{d}_{0\text{bf}} \approx 0.4256$. We observed no convergence for the values of $\bar{d}_0 > \bar{d}_{0\text{bf}}$.

Direct application of the scheme in Eq. (6) demonstrates convergence only for the lower branch of solutions, and does not allow one to find the upper branch of solutions. In order to find the solutions from the upper branch we study the spectrum of the N and modify the map.

4. Convergence of the map N

In order to understand the convergence of the iterative procedure described in Eq. (6) we analyze the spectrum of $N_{\bar{d}_0}$ near a fixed point. In the neighborhood of the fixed point φ_{fp} the map $N_{\bar{d}_0}$ is approximated by the linear operator K :

$$N(\varphi_{\text{fp}} + \Psi) = \varphi_{\text{fp}} + K(\Psi) + \mathcal{O}(\Psi^2). \quad (8)$$

Here the operator K lacks the complex structure and should be viewed as a linear operator over the field of real numbers acting on a real vector space consisting of functions $\text{Re } \Psi$ and $\text{Im } \Psi$. Let the finite set $\{\mu_i\}$, $\{|\phi_i\rangle\}$, and $\{\langle\phi_i|\}$ correspond to eigenvalues, right eigenvectors and left eigenvectors of \hat{K} , the discretized version of K . Right away we see that there is an eigenvalue 1 corresponding to a constant phase shift of any fixed point. This eigenvector does not affect the convergence since Eq. (7) is unaffected by the constant phase shift. Therefore, we introduce the sets $\{\tilde{\mu}_i\} = \{\mu_i\} \setminus 1$ and $\{|\tilde{\phi}_i\rangle\} = \{|\phi_i\rangle\} \setminus |\phi_{\mu=1}\rangle$, $\{\langle\tilde{\phi}_i|\} = \{\langle\phi_i|\} \setminus \langle\phi_{\mu=1}|$ where we have removed the above eigenvector and the corresponding eigenvalue. Furthermore, we assume that if $i < j$ than $|\tilde{\mu}_i| \geq |\tilde{\mu}_j|$, so that $\tilde{\mu}_1$ has maximal magnitude. The following iterative procedure is used to obtain the N th eigenfunction

$$|\tilde{\phi}_N\rangle = \lim_{n \rightarrow \infty} \Psi_n, \quad \text{where } \Psi_{n+1} = \frac{\hat{K}(\Psi_n) - \sum_{j=1}^{N-1} \langle\tilde{\phi}_j|\hat{K}(\Psi_n)\rangle|\tilde{\phi}_j\rangle}{\int |\Psi_n|^2 d\Omega} \quad (9)$$

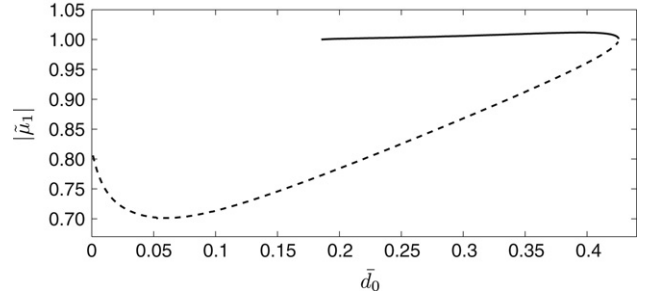


Fig. 2. A plot of largest eigenvalue of \hat{K} as a function of time \bar{d}_0 at the upper branch solutions (solid) and at the lower branch solutions (dashed).

where $\langle\tilde{\phi}_j|$ is a dual vector of $|\tilde{\phi}_j\rangle$, satisfying $\langle\tilde{\phi}_j|\tilde{\phi}_k\rangle = \delta_{jk}$ (here δ_{jk} is a Kronecker symbol). We assume here that initial function Ψ_0 has nonzero projection onto N th eigenfunction. At each step of this procedure the largest $N - 1$ modes are projected out of Ψ_n and in the limit as the number of iterations n goes to infinity the next largest mode is the only one that survives. The contribution from the M th vector ($M > N$) dies out as $(\tilde{\mu}_M/\tilde{\mu}_N)^n$.

In order to perform the procedure described in Eq. (9) we use the explicit expression for the operator \hat{K}

$$\hat{K}(\Psi) = 1.5\varphi_{\text{fp}} \int \text{Re}[\varphi_{\text{fp}}^*(\Psi - L(\Psi))] d\Omega \bigg/ \int |\varphi_{\text{fp}}|^2 d\Omega + L(\Psi) \quad (10)$$

$$\text{and } L(\Psi) \equiv \int \frac{\sin(\Delta/2)}{\Delta/2} (\varphi_{\text{fp}}(\Omega_1)\varphi_{\text{fp}}(\Omega_2)\Psi^*(\Omega_3) + 2\varphi_{\text{fp}}(\Omega_1)\Psi(\Omega_2)\varphi_{\text{fp}}^*(\Omega_3)) \frac{\delta(\Omega_1 + \Omega_2 - \Omega_3 - \Omega)}{1 + \bar{d}_0\Omega^2} d\bar{\Omega}$$

here $d\bar{\Omega} = d\Omega_1 d\Omega_2 d\Omega_3$. The operator \hat{K} is not self-adjoint, therefore, its left and right eigenvectors are different. We obtain the the left eigenvectors of the operator \hat{K} by studying the right eigenvectors of the operator \hat{K}^\dagger

$$\hat{K}^\dagger(\xi) = L^\dagger(\xi) - \xi + L^\dagger(\xi)$$

$$\xi \equiv 1.5\varphi_{\text{fp}} \int \text{Re}[\varphi_{\text{fp}}^*\xi] d\Omega \bigg/ \int |\varphi_{\text{fp}}|^2 d\Omega$$

$$L^\dagger(\xi) = \int \frac{\sin(\Delta_+/2)}{\Delta_+/2} \varphi_{\text{fp}}(\Omega_1)\varphi_{\text{fp}}(\Omega_2)\xi^*(\Omega_3) \times \frac{\delta(\Omega_1 + \Omega_2 - \Omega_3 - \Omega)}{1 + \bar{d}_0\Omega_3^2} d\bar{\Omega} \quad (11)$$

$$+ \int \frac{\sin(\Delta_-/2)}{\Delta_-/2} 2\varphi_{\text{fp}}(\Omega_1)\xi(\Omega_2)\varphi_{\text{fp}}^*(\Omega_3) \times \frac{\delta(\Omega_1 - \Omega_2 - \Omega_3 + \Omega)}{1 + \bar{d}_0\Omega_2^2} d\bar{\Omega}$$

$$\Delta_\pm \equiv \Omega_1^2 \pm \Omega_2^2 - \Omega_3^2 \mp \Omega^2.$$

Fig. 2 shows how the largest magnitude eigenvalue of the operator \hat{K} depends on \bar{d}_0 . Here the dashed line corresponds to the lower branch of solutions and the solid line corresponds to the upper branch of solutions. Since for all values of \bar{d}_0 the largest eigenvalue of \hat{K} at the lower branch solutions is less than 1 the map N is contractive. Therefore as long as we are close enough to the fixed point the iterations will converge. The situation is different for the upper branch of solutions. As clearly shown on Fig. 3 for all values of \bar{d}_0 the largest eigenvalue is larger than 1 and therefore the map is not contractive.

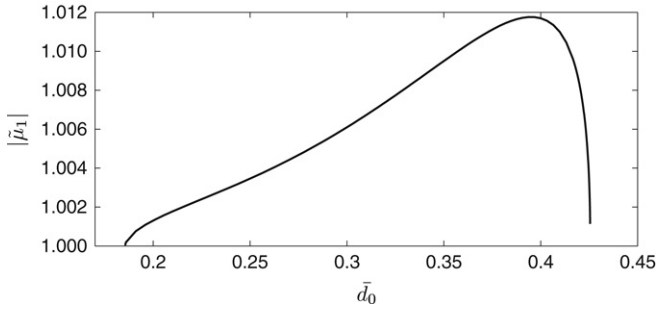


Fig. 3. Plot of $|\tilde{\mu}_1|$ vs \tilde{d}_0 for the upper branch only. The graph exhibits vertical behavior near $\tilde{d}_0 \approx 0.4256$ and near $\tilde{d}_0 \approx 0.1856$. In the first case this behavior is due to bifurcation.

5. Construction of a contractive map

We construct a map that retains the same fixed points as $N_{\tilde{d}_0}(\varphi)$ in Eq. (6) and at the same time a map that is contractive in the neighborhood of the upper branch fixed points.

Consider a polynomial $\mathbb{P}(x) = \sum_{j=0}^p b_j x^j$ and use it to construct a new map P:

$$P(\varphi) \equiv \mathbb{P}(N(\varphi)) = \sum_{j=0}^p b_j N^j(\varphi) \quad (12)$$

$$N^0(\varphi) = \varphi, \quad N^j = N(N(\dots N(\varphi))) \quad j \text{ times.}$$

In the neighborhood of a fixed point this operator has the following linearization

$$\begin{aligned} P(\varphi_{\text{fp}} + \psi) &= P\left(\varphi_{\text{fp}} + \sum_i a_i \tilde{\phi}_i\right) \\ &= \sum_{j=0}^p b_j \left(\varphi_{\text{fp}} + K^j \left(\sum_i a_i \tilde{\phi}_i\right)\right) \\ &= \sum_{j=0}^p b_j \left(\varphi_{\text{fp}} + \sum_i a_i \tilde{\mu}_i^j \tilde{\phi}_i\right) \\ &= \varphi_{\text{fp}} \sum_{j=0}^p b_j + \sum_i a_i \left(\sum_{j=0}^p b_j \tilde{\mu}_i^j\right) \tilde{\phi}_i. \end{aligned} \quad (13)$$

We choose the values of b_j so that the $\sum b_j = 1$. Due to this condition the new map retains the same fixed point as N . Thus after n iterations we have

$$P^n(\varphi_{\text{fp}} + \psi) = \varphi_{\text{fp}} + \sum_i a_i \{\mathbb{P}(\tilde{\mu}_i)\}^n \tilde{\phi}_i. \quad (14)$$

We choose the coefficients of the polynomial b_i in such a manner that the condition $\max\{|\mathbb{P}(\tilde{\mu}_i)|\} < 1$ is satisfied. According to Eq. (14) each mode decays exponentially, and the smaller $\max\{|\mathbb{P}(\tilde{\mu}_i)|\}$ is, the faster the convergence.

Our approach is a modification of the technique considered in [19], where only first order polynomials were needed. In our case we found a 5th order polynomial that fit our needs. The coefficients of the polynomial could be optimized further for the faster convergence. This issue is discussed in the matrix Chebyshev approximation problem [20–22].

Fig. 4 shows the 10 largest eigenvalues of K at the fixed point $\varphi_{\tilde{d}_0=0.4}^{\text{upper}}$ found numerically using the method in Eq. (9). This is a typical picture for all upper branch fixed points. This computation shows that the imaginary part of these eigenvalues is either very small or zero. The real part of the first 10 eigenvalues lies between 0 and 1.012 and all other eigenvalues lie in the shaded area. There are two key features of the spectrum that should be

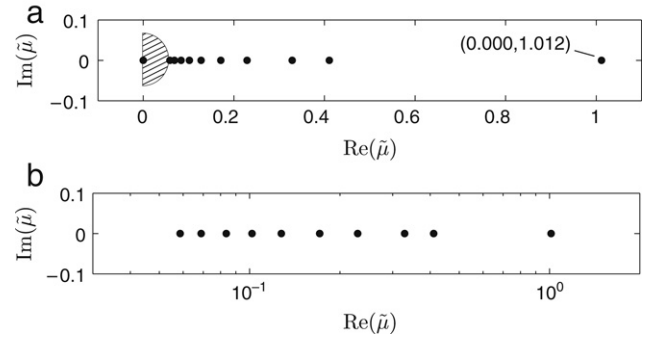


Fig. 4. A plot of the imaginary part of eigenvalue versus the real part. Plotted first 10 eigenvalues of operator K at $\varphi_{\tilde{d}_0=0.4}^{\text{upper}}$. In subfigure (a) the shaded region defines the part of space where the rest of eigenvalues lay. In subfigure (b) the real part is plotted on logarithmic scale.

emphasized. First, $\tilde{\mu}_1$ is extremely close to 1. As shown on Fig. 3 this feature is shared by all of the upper branch solutions. Second, as demonstrated by Fig. 5 the following inequality takes place: $|\tilde{\mu}_1 - 1| \ll |1 - \tilde{\mu}_2|$. The decay of the first mode is proportional to $\mathbb{P}(\tilde{\mu}_1)^n$ where n is the number of iterations performed, therefore, to make the convergence of this mode as fast as possible we choose a polynomial with a derivative at $(1, 1)$ near a value of $-1/(\tilde{\mu}_1 - 1)$. Due to the first feature $\tilde{\mu}_1 - 1$ being very small, this implies fast growth of the polynomial to the left of the point $(1, 1)$. However, due to the second feature of the spectrum such a behavior is not problematic, since there is plenty of room for the polynomial to return close to zero. Thus, consider the polynomial presented in the Fig. 6 and defined as

$$\mathbb{P}(x) = \prod_{i=1}^p (x - r_i) / \prod_{i=1}^p (1 - r_i) \quad (15)$$

and let $r_1 = 0.0, r_2 = 0.1, r_3 = 0.3, r_4 = 0.46, r_5 = 1.01$.

This is a fifth order polynomial with $|\mathbb{P}(\tilde{\mu}_i)| < 1$ and $\mathbb{P}(1) = 1$. Following the earlier discussion we can see that this polynomial does in fact has large slope at $(1, 1)$, and yet there is enough room for the values to drop back down as x approaches $\tilde{\mu}_2$. Also note that this is only a fifth degree polynomial, and therefore one iteration of $\mathbb{P}(N)$ requires only five iterations of N .

To catch the solution on the upper branch we have to be as close as possible to the solution before we start our iterative process. Before computing the upper branch, the lower one was obtained. Because of the bifurcation structure it is natural to expect that the function $2\varphi_{\tilde{d}_0\text{bf}} - \varphi_{\tilde{d}_0}$ could serve as a good starting seed for the upper branch solution at \tilde{d}_0 . Even with simple iterations (without the polynomial deformation of the map in order to make it contractive) it was clear that there exists another branch of solutions, as for the first few iteration, the residual (see Eq. (7)) was quickly decreasing (diverging in the long run.)

The behavior of $\tilde{\mu}_1$ illustrated in Fig. 3 suggests that there is another bifurcation point with $\tilde{d}_0\text{bf} \approx 0.18$ and yet another branch of antisymmetric bisoliton solutions. There is strong evidence of that from applying the shooting method using $2\varphi_{\tilde{d}_0\text{bf}} - \varphi_{\tilde{d}_0}$ from the computed upper branch.

6. Direct simulation of bisoliton propagation

As a demonstration that the computed solutions of the averaged Eq. (4) are solitary wave approximations of the Eq. (1) we perform a direct simulation of (1) with the following initial condition

$$u_0(t) \equiv u(t, L/4) = 2\pi\sqrt{PF}^{-1} \left[\varphi_{\tilde{d}_0}(\Omega) \right] \Big|_{t=t/\sqrt{Ld_1/2}} \quad (16)$$

